Journal of proteome research

Article

pubs.acs.org/jpr

Robust, Sensitive, and Automated Phosphopeptide Enrichment Optimized for Low Sample Amounts Applied to Primary Hippocampal Neurons

Harm Post,[†,‡,∥] Renske Penning,[†,‡,∥] Martin A. Fitzpatrick,[†,‡] Luc B. Garrigues,[†,‡] W. Wu,[†,‡] Harold D. MacGillavry,[§] Casper C. Hoogenraad,[§] Albert J. R. Heck,[†,‡] and A. F. Maarten Altelaar*[,†,‡]

[†]Biomolecular Mass Spectrometry and Proteomics, Bijvoet Center for Biomolecular Research and Utrecht Institute for Pharmaceutical Sciences, Utrecht University, Padualaan 8, 3584 CH Utrecht, The Netherlands

[‡]Netherlands Proteomics Centre, Padualaan 8, 3584 CH Utrecht, The Netherlands

[§]Cell Biology, Department of Biology, Faculty of Science, Utrecht University, 3584 CH Utrecht, The Netherlands

Supporting Information

ABSTRACT: Because of the low stoichiometry of protein phosphorylation, targeted enrichment prior to LC−MS/MS analysis is still essential. The trend in phosphoproteome analysis is shifting toward an increasing number of biological replicates per experiment, ideally starting from very low sample amounts, placing new demands on enrichment protocols to make them less labor-intensive, more sensitive, and less prone to variability. Here we assessed an automated enrichment protocol using Fe(III)-IMAC cartridges on an AssayMAP Bravo platform to meet these demands. The automated Fe(III)-IMAC-based enrichment workflow proved to be more effective when compared to a TiO_2-based enrichment using the same platform and a manual Ti(IV)-IMAC-based enrichment workflow. As initial samples, a dilution series of both human HeLa cell and primary rat hippocampal neuron lysates was used, going down to 0.1 μg of peptide starting material. The optimized workflow proved to be efficient, sensitive, and reproducible, identifying, localizing, and quantifying thousands of phosphosites from just micrograms of starting material. To further test the automated workflow in genuine biological applications, we monitored EGF-induced signaling in hippocampal neurons, starting with only 200 000 primary cells, resulting in ∼50 μg of protein material. This revealed a comprehensive phosphoproteome, showing regulation of multiple members of the MAPK pathway and reduced phosphorylation status of two glutamate receptors involved in synaptic plasticity.

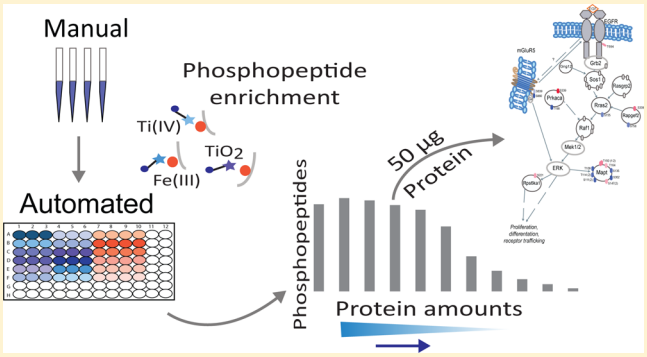

KEYWORDS: *phosphoproteomics, quantification, Fe(III)-IMAC, Ti(IV)-IMAC, TiO_2, BRAVO AssayMap, phosphopeptide enrichment, sensitivity, EGF, hippocampal neurons*

INTRODUCTION

Protein function within the cellular environment is in part defined by posttranslational modifications (PTMs). Phosphorylation is a key component of cellular signal transduction, and it plays a critical role in many biological processes, where aberrant protein phosphorylation is often correlated with disease.[1−6] This makes phosphorylation one of the best studied PTMs, most commonly achieved using high-resolution mass spectrometry (MS) because of its ability to localize phosphosites to specific amino acids.[7,8] Unfortunately, as phosphorylation is often of low stoichiometry and covers a high dynamic range, characterization by MS is not straightforward.[2,9,10]

In the past decade, a multitude of technological developments have substantially advanced large-scale phosphoproteome profiling.[11−13] Most methods employ a targeted enrichment of phosphorylated peptides (phosphopeptides) prior to LC−MS/MS analysis using ion exchange chromatography,[2,14−16] phospho (motif) specific antibodies,[17,18] metal oxide surfaces (TiO_2),[19,20] or chelation.[21,22] Recently, a new generation of chelation materials has allowed excellent and robust enrichment of phosphopeptides. These monodisperse microsphere-based immobilized metal ion affinity chromatography (IMAC) resins incorporate flexible linkers that are terminated by phosphonate groups that chelate metal ions. These materials offer superior coordination of phosphopeptides in a robust fashion, tolerating the use of harsh solvent conditions. Various metal ions including Ga(II),[22,23] Ti-(IV),[24,25] and Fe(III)[21] have been used in these IMAC-based phosphopeptide enrichment strategies.

Received: August 17, 2016
Published: November 28, 2016

DOI: 10.1021/acs.jproteome.6b00753
J. Proteome Res. 2017, 16, 728−737

Because of the combination of low stoichiometry of phosphopeptides and the resulting need for enrichment, the amount of starting material required for the recovery of a comprehensive phosphoproteome has so far been relatively large, especially when compared with standard proteome analysis. This induces a problem in the analysis of primary cell cultures, microdissected cells, organoids, or tissue samples, where available sample quantities are typically low. With increasingly complex experiments (i.e., more time-points, more biological replicates), manually conducted experiments can become very labor intensive. Although we previously already showed that Ti(IV)-IMAC-based enrichment can be qualitatively and quantitatively reproducible,[26] the many steps in the protocol make it sensitive to sample variability. To enhance reproducibility in large experimental setups and minimize sample losses, the total sample handling and variability should ideally be further reduced. One approach to achieve this is through miniaturization and automation, which allows for processing of multiple samples in parallel, resulting in increased efficiency and reduced variability.

Last year, EasyPhos was developed as a first approach to perform phosphoproteomics in an automated workflow.[27] While it revealed the potential of automated phosphopeptide enrichment, relatively large amounts of protein input material (1 mg) were used. More recently Abelin et al.[28] demonstrated that a combination of Fe(III)-IMAC cartridges and an automated setup, the Agilent AssayMap Bravo Platform, enables the identification of over 10 000 unique phosphosites, combining three cell lines treated with 27 compounds (including DMSO). However, also these experiments were conducted using relatively large amounts of protein material (0.5 mg). Taking the latter Fe(III)-IMAC-based automated workflow as starting point, we here explored whether this workflow could also be used when starting with up to 5000 times lower amounts of protein digest and thus applied to challenging biological samples such as primary rat hippocampal neurons.

MATERIALS AND METHODS

Cell Cultures

HeLa cells were grown in Dulbeco's modified Eagle's medium (DMEM) supplemented with 10% fetal bovine serum and 10 mM glutamine (all from Lonza, Braine-l'Alleud, Belgium). Six hours before harvesting, the medium was replaced by fresh medium. Cells were harvested and the cell pellets were immediately washed two times with phosphate-buffered saline buffer (PBS) and stored at −80 °C until further usage.

Dissociated hippocampal neuron cultures were prepared from embryonic day 18 rats of either sex. Cells were plated at a density of 200 000 per well and treated as described before.[29] The hippocampal cultures were grown in neurobasal medium (Thermo Scientific) supplemented with B27, 0.5 μM glutamine, and penicillin/streptomycin. At days 14 and 15 after plating, the cells were stimulated with either vehicle or 10 ng/mL epidermal growth factor (EGF, Sigma-Aldrich) for 20 min. Cells were not starved before the addition of EGF. Cells were harvested and washed with PBS and stored at −80 °C until further usage.

Protein Lysis and Digestion

Cells were lysed, reduced, and alkylated in lysis buffer (1% sodium deoxycholate (SDC), 10 mM tris(2-carboxyethyl)-phosphinehydrochloride (TCEP)), 40 mM chloroacetamide (CAA), and 100 mM TRIS, pH 8.0 supplemented with phosphotase inhibitor (PhosSTOP, Roche) and protease inhibitor (cOmplete mini EDTA-free, Roche). A Bradford protein assay was performed three times to quantify protein amount. Cells were heated for 5 min at 95 °C, sonicated with a Bioruptor Plus (Diagenode) for 15 cycles of 30 s, and diluted 1:10 with 50 mM ammoniumbicarbonate, pH 8.0. Proteins were digested overnight at 37 °C with trypsin (Sigma-Aldrich) with an enzyme/substrate ratio of 1:50 and lysyl endopeptidase (Lys-C, Wako) with an enzyme/substrate ratio of 1:75. SDC was precipitated with 2% formic acid (FA) and samples were desalted using Sep-Pak C18 cartridges (Waters) and eluted with 80% acetonitrile (ACN)/0.1% trifluoroacetic acid (TFA) and directly subjected to phosphopeptide enrichment or dried down and stored at −80 °C until further use.

Phosphorylated Peptide Enrichment

Manual Ti(IV)-IMAC-Based Workflow. Phosphopeptide enrichment was performed as described as before.[25] In brief, 500 μg Ti(IV)-beads were packed into a GELoader microtip column and washed with methanol and loading buffer (80% (ACN)/6% TFA). Samples were dissolved in loading buffer and loaded onto the beads. Columns were washed with 50% ACN/0.5% TFA in 200 mM NaCl and 50% ACN/0.1% TFA, and phosphopeptides were eluted with 10% ammonia and 80% ACN/2%FA directly into 10% FA. Samples were dried down and stored at −80 °C until LC−MS/MS analysis.

Automated TiO_2 and Fe(III)-IMAC-Based Workflows. Phosphorylated peptides were enriched using either TiO_2 or Fe(III)-NTA 5 μL (Agilent technologies) in an automated fashion using the AssayMAP Bravo Platform (Agilent Technologies). TiO_2 columns were primed with 250 μL of 5% ammonia/15% ACN and equilibrated with loading buffer (50% ACN/2% TFA). Samples were dissolved in 200 μL of loading buffer and loaded onto the column. The cartridges were washed with 250 μL of loading buffer, and the phosphorylated peptides were eluted with 25 μL of 5% ammonia directly into 25 μL of 10% formic acid and dried down. Fe(III)-NTA cartridges were primed with 250 μL of 0.1% TFA in ACN and equilibrated with 250 μL of loading buffer (80% ACN/0.1% TFA). Samples were dissolved in 200 μL of loading buffer and loaded onto the cartridge. The columns were washed with 250 μL of loading buffer, and the phosphorylated peptides were eluted with 25 μL of 1% ammonia directly into 25 μL of 10% formic acid. Samples were dried down and stored in −80 °C until subjected to LC−MS/MS.

Mass Spectrometry: RP-nanoLC−MS/MS

The data were acquired using an UHPLC 1290 system (Agilent) coupled to an Orbitrap Q Exactive Plus mass spectrometer (Thermo Scientific). Peptides were first trapped (Dr Maisch Reprosil C18, 3 μm, 2 cm × 100 μm) before being separated on an analytical column (Agilent Poroshell EC-C18, 2.7 μm, 50 cm × 75 μm). Trapping was performed for 10 min in solvent A (0.1 M acetic acid in water), and the gradient was as follows: 4−8% solvent B (0.1 M acetic acid in 80% ACN) in 2 min, 8−24% in 71 min, 24−35% in 16 min, 35−60% in 7 min, 60−100% in 2 min, and finally 100% for 1 min. Flow was passively split to 300 nL min^{-1}. The mass spectrometer was operated in data-dependent mode. Full-scan MS spectra from m/z 375−1600 were acquired at a resolution of 35 000 at m/z 400 after accumulation to a target value of 3×10^6. Up to 10 most intense precursor ions were selected for fragmentation. HCD fragmentation was performed at normalized collision

DOI: 10.1021/acs.jproteome.6b00753
J. Proteome Res. 2017, 16, 728−737

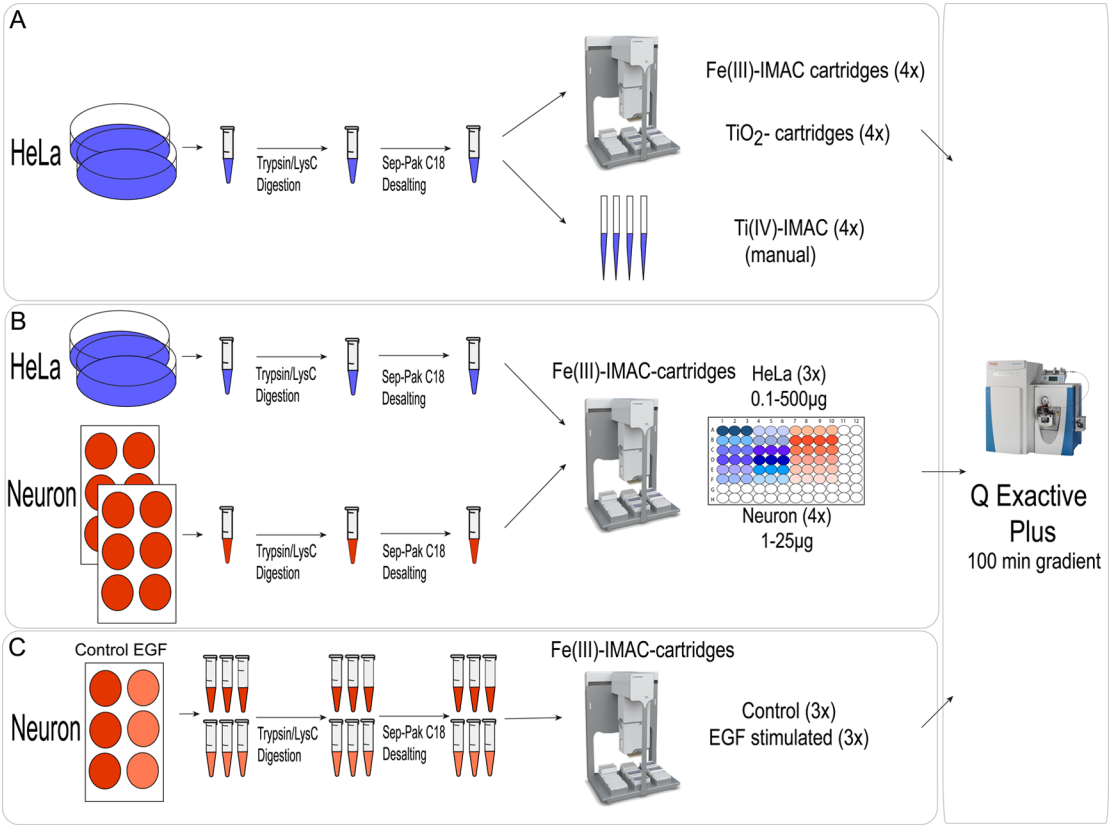

Figure 1. Overview of employed workflows for sensitive phosphoproteome analysis. (A) Assessment of performance of three enrichment strategies, namely, manually using Ti(IV)-IMAC loaded tips or automated using the Bravo AssayMAP Platform with either Fe(III)-IMAC or TiO_2-loaded cartridges. (B) Phosphoproteome analysis, using the automated Fe(III)-IMAC-based workflow, of varying amounts of HeLa digest (0.1−500 μg) and Rat hippocampal neuron digests (1−25 μg). (C) Phosphopeptide enrichment, using the automated Fe(III)-IMAC-based workflow, of rat hippocampal neurons digests stimulated with EGF or vehicle for 20 min. All samples resulting from the phosphopeptide enrichments were analyzed via a single LC−MS/MS run using a 100 min gradient on a Q Exactive Plus. Bravo AssayMAP Platform image courtesy of Agilent Technologies, Inc. Permission for the use of the image of the Thermo Scientific Q Exactive Plus Hybrid Quadrupole-Orbitrap Mass Spectrometer has been granted by Thermo Fisher Scientific.

energy of 25% after the accumulation to a target value of 5×10^4. MS/MS was acquired at a resolution of 17 500.

Data Analysis

Raw files were processed using MaxQuant (version 1.5.3.30). The database search was performed against the human Swissprot database (version June 25, 2015) or the *Rattus norvegicus* Ensemble database (version March 12, 2016) using Andromeda as search engine. Cysteine carbamidomethylation was set as a fixed modification and methionine oxidation, protein N-term acetylation, and phosphorylation of serine, threonine, and tyrosine were set as variable modifications. Trypsin was specified as enzyme and up to two miss cleavages were allowed. Filtering was done at 1% false discovery rate (FDR) at the protein and peptide level. Label-free quantification (LFQ) was performed, and "match between runs" was enabled.

Quantified data were processed and analyzed using a custom Python package (PaDuA) to remove potential contaminants and reverse peptides, filtered for localization probability >0.75, log2-transformed and normalized to column median as per standard methods. Statistical analysis, including principal component analysis (PCA), correlation, and clustering, were performed on the processed data.

RESULTS AND DISCUSSION

Our aim was to test the performance of the AssayMAP Bravo Platform automated phosphopeptide enrichment workflow for high-throughput phosphoproteome analysis using small amounts of starting material. We first evaluated the performance of the manufacturer-supplied TiO_2 and Fe(III)-IMAC cartridges on the Agilent AssayMAP Bravo Platform against our own established manual Ti(IV)-IMAC-based phosphopeptide workflow, as previously described[25,26] (Figure 1A). After lysis of HeLa cells using the SDC protocol,[30] protein extracts were digested using Lys-C and trypsin, and 200 μg of the resulting peptides was subjected to either TiO_2- or Fe(III)-IMAC based automated phosphopeptide enrichment or manual enrichment using the Ti(IV)-IMAC-based workflow. After enrichment, the samples were subjected to a single LC−MS/MS run with a 100 min effective gradient on a Q Exactive Plus (where all phosphopeptide enrichments are described below). As shown in Figure 2A, the Fe(III)-IMAC- and Ti(IV)-IMAC-based workflows outperformed the TiO_2-based workflow, with 22−34% more uniquely identified phosphosites in four consecutive enrichments. On average, 7672 unique phosphosites were identified in a single enrichment using Ti(IV)-IMAC, 8110 phosphosites using Fe(III)-IMAC, and 5980 phosphosites in the TiO_2-based enrichments. The enrichments using Fe(III)-IMAC and Ti(IV)-IMAC were highly specific (>90%) (Figure

DOI: 10.1021/acs.jproteome.6b00753
J. Proteome Res. 2017, 16, 728−737

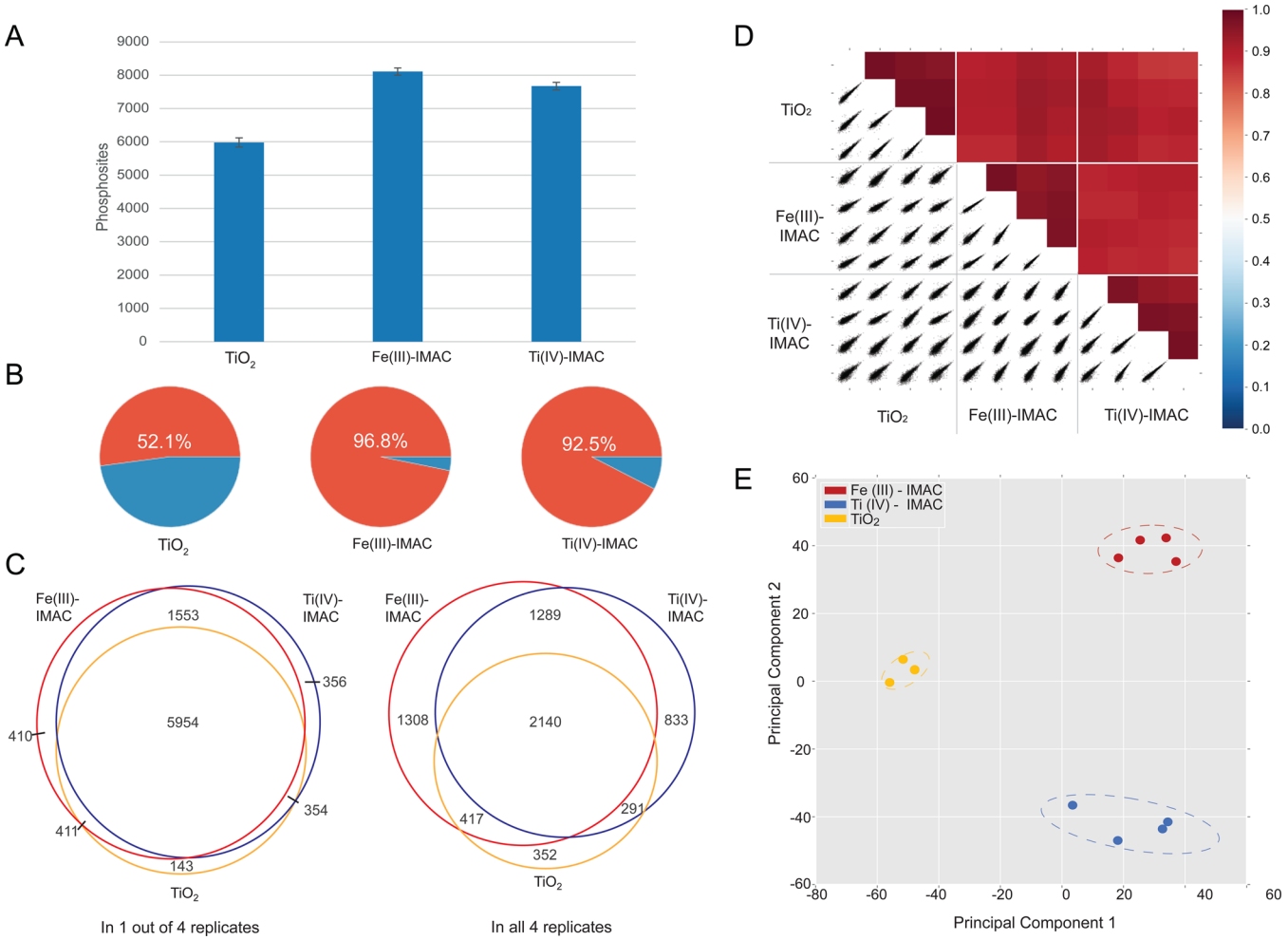

Figure 2. Assessment of performance and characteristics of phosphopeptide enrichment strategies. Three strategies were comparatively assessed, namely, a manual approach using Ti(IV)-IMAC loaded tips or automated using the Bravo AssayMAP with either Fe(III)-IMAC or TiO_2 loaded cartridges, using 200 μg of HeLa digest as input. (A) Average number of identified phosphosites in a single LC−MS/MS run performed in quadruplicate for the three different enrichment strategies. The TiO_2-loaded cartridges systematically underperform (for reasons highlighted in the text), while the automated Fe(III)-IMAC approach performs at least as well as the more labor intensive manual workflow using Ti(IV)-IMAC loaded tips. (B) Percentages of identified phosphopeptides compared with the total number of identified peptides for the applied enrichment strategies, revealing a highly specific phosphopeptide enrichment efficiency for Ti(IV)-IMAC and Fe(III)-IMAC. The lower efficiency of ∼50% for TiO_2 is further discussed in the text. (C) Venn diagrams displaying the overlap between the three phosphopeptide enrichment methods in identified phosphosites observed in one out of four replicates and in all four replicates, showing a good overlap in identifications between the different methods. (D) Comparison of label-free quantification of phosphopeptides within one enrichment workflow and in between workflows. The heatmap shows the Pearson correlations and correlation plots for the different replicates. Overall, the different phosphopeptide enrichment experiments reveal a good correlation, with the highest values observed for data gathered within one single workflow. (E) Different phosphopeptide enrichment workflows lead to distinctive phosphoproteomes. PCA analysis of the three different used enrichment methods reveals strong clustering of replicate enrichments using the same workflow, which can be distinguished from measurements by alternative workflows.

2B), while TiO_2 displayed an enrichment specificity of just 50%. The overall lower performance of the TiO_2 automated workflow on the AssayMAP Bravo Platform was unexpected, as we recently demonstrated equal performance of TiO_2 and Ti(IV)-IMAC in a manual approach[9] and can most likely be attributed to the use of nonideal buffer conditions compared with our manual approach. The high concentration of TFA in the buffers used for the manual approach is not compatible with the cartridges in the AssayMAP Bravo Platform. The performance of the TiO_2 cartridges can likely be further improved by applying different buffer conditions and with additives like glutamic acid.[31] To evaluate differences in enrichment properties between the methods, the percentages of mono-, di-, and multiply phosphorylation and the percentage of S, T, and Y enrichment are evaluated in Figure S1. As expected, the different methods enrich phosphopeptides with very similar characteristics.

For our quantitative analysis we selected all Class I phosphosites (site localization probability ≥0.75) being detected in at least two replicates, cumulatively resulting in 6408 phosphosites for Ti(IV)-IMAC, 6973 for Fe(III)-IMAC, and 4756 for TiO_2. This stringent filtering was used for all below reported analyses. The overlap in enriched phosphopeptides between the different methods was high (Figure 2C), with 91% overlap between Ti(IV)-IMAC and Fe(III)-IMAC, 84% between Fe(III)-IMAC and TiO_2, 84% between Ti(IV)-IMAC and TiO_2, and 76% found for all three methods in at least one out of four replicates per method.

Previously we showed that the manual approach using Ti(IV)-IMAC is reproducible and can be used for quantitative

DOI: 10.1021/acs.jproteome.6b00753
J. Proteome Res. 2017, 16, 728−737

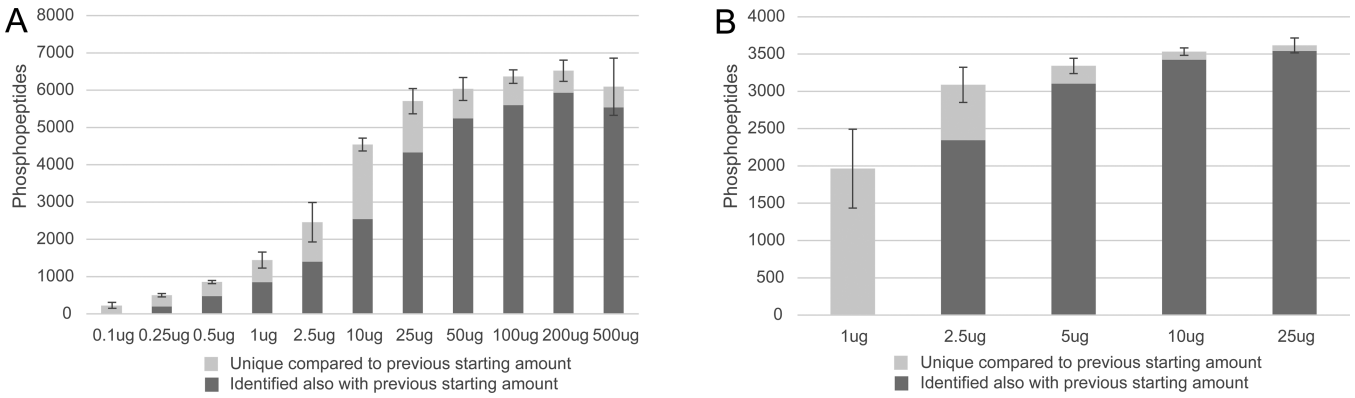

Figure 3. Sensitivity of the automated phosphoproteome analysis. Number of phosphopeptides identified, using the automated Fe(III)-IMAC workflow, from various amounts of starting material of HeLa digest (A) and primary rat (B) hippocampal neuron digest. The data show an increasing number of identifications with higher amount of starting material up to 200 μg for the HeLa digest. Light-gray regions indicate the number of phosphopeptides also identified at lower concentrations, showing gain in phosphopeptide identification numbers by using more protein digest as input for phosphopeptide enrichment.

phosphoproteome analysis using label-free quantification based on peptide ion intensities.[26] Here we evaluated whether the automated workflows (using either Fe(III)-IMAC or TiO_2) can also be used for quantitative phosphoproteome profiling and whether this quantitation is enrichment workflow-dependent. We thus compared, focusing on the overlapping phosphopeptides detected in all enrichments, the phosphopeptide ion intensities. Although the overall correlation between experiments is very good, the data displayed in Figure 2D reveal that the correlation is best when a single enrichment method is used and weaker when we, for instance, compare data from a TiO_2 enrichment with a Fe(III)-IMAC-based enrichment. This behavior is further exemplified by a principal component analysis (Figure 2E), which revealed the replicate enrichments for each workflow cluster, together indicating strong reproducibility, with Fe(III)-IMAC and Ti(IV)-IMAC being most similar.

On the basis of these results, we were especially satisfied with the performance of the Fe(III)-IMAC-based automated platform and decided to further characterize and validate the performance of this approach and to not further optimize the use of TiO_2 cartridges. As shown above, the Fe(III)-IMAC cartridges showed excellent performance using 200 μg of HeLa digest. However, in many biological experiments the amount of available protein material can be considerably smaller. Thus next we assessed the performance of the Fe(III)-IMAC cartridges using decreasing amounts of HeLa digest (0.1−500 μg), making use of a dilution series (Figure 1B). As expected and displayed in Figure 3A, the number of identified phosphopeptides was lower when starting with very low amounts of input material. Remarkably though, starting with only 100 ng of HeLa digest, we were still able to identify 215 unique phosphopeptides; with 1 μg, this increased to 1443 unique phosphopeptides; and with 10 μg of HeLa digest, 4541 unique phosphopeptides were identified. Cumulatively, the replicate enrichments of 100 ng resulted in 319 unique phosphopeptides bearing 415 class I phosphosites in at least two replicates, 1 μg in 1903 unique phosphopeptides and 1694 phosphosites, and 10 μg in 5726 unique phosphopeptides and 4324 phosphosites. Using 200 μg of input material resulted in an optimal performance of the Fe(III)-IMAC cartridges in terms of identified phosphopeptides with over 8269 unique phosphopeptides being identified and 5697 class I phosphosites quantified in at least two replicates using a single 100 min LC−MS/MS analysis per enrichment. The qualitative reproducibility was high for all enrichment amounts with an overlap of >65% between consecutive enrichments (see Figure S2). The reproducibility decreased once <1 μg of HeLa digest was used. Next to the qualitative, the quantitative reproducibility was also very high between consecutive HeLa digest enrichments when using the same amount of starting material, with an average correlation of $R = 0.87$, comparable to the correlation observed in technical replicate LC−MS/MS runs.[26,27] Interestingly, the Pearson correlation remained high when, after normalization, the different amounts of starting material were compared (Figure S2A). This high correlation remained when the "match between runs" function in Max Quant was disabled, ensuring reproducibility of the results (Figure S2B). Two relative outliers were observed, namely, the two extreme cases in the amount of starting material, 0.1 μg and 500 μg in the HeLa digest. It may not be surprising that the correlation decreased most for the 0.1 μg samples, where the MS signal-to-noise is poorest. The lower correlation observed when starting with 500 μg of HeLa digest can most likely be explained by overloading of the cartridge, although identification rates were still high. Therefore, we evaluated the linearity of phosphopeptide enrichment using the HeLa samples.[32] As plotted in Figure S3, samples display good linearity up to 100 μg of protein used, indicating that with higher protein amounts the maximum capacity of the cartridges is reached, causing an increase in enrichment variation. Interestingly, Figure 3A shows that the vast majority of phosphopeptides identified in the 200 μg HeLa sample could already be identified in the analysis using lower sample amounts.

Evidently, in the case of lab-cultured HeLa cell lines the sample quantity is not likely a limiting factor. Therefore, we also analyzed the phosphoproteome of a more applicable biological system using rat primary hippocampal neurons. These primary neuronal cells are typically plated in six-well format with a density of 200 000 cells per well, leading to ~50 μg of proteinaceous material per sample. Because of the specialized function of neuronal cells, we hypothesized a larger dynamic range in protein expression and relatively lower phosphorylation levels compared with the HeLa cell digests. We tested the Fe(III)-IMAC-based automated enrichment method on these primary neurons in triplicate using again a

DOI: 10.1021/acs.jproteome.6b00753
J. Proteome Res. 2017, 16, 728−737

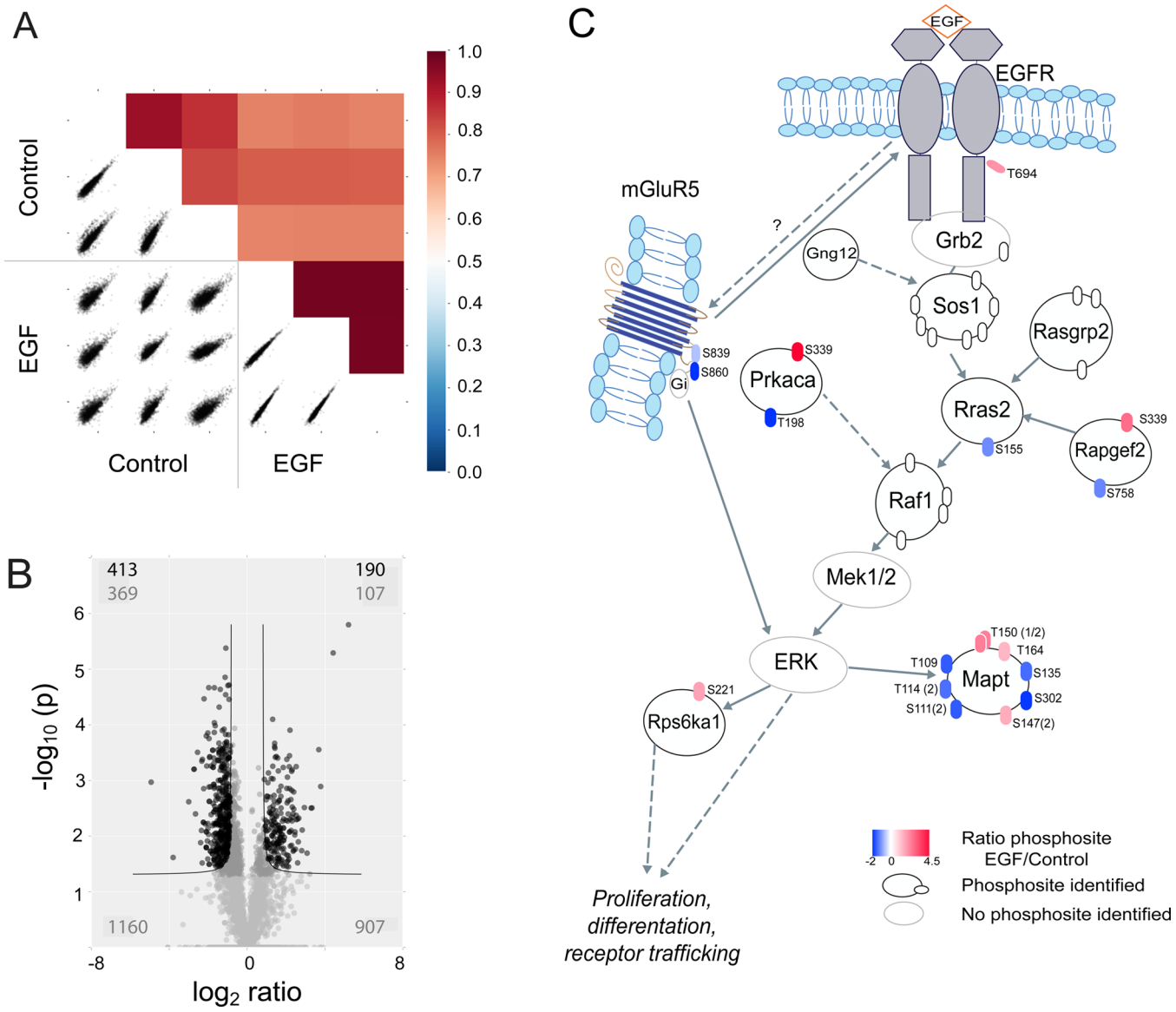

Figure 4. Label-free phosphoproteome analysis of Rat hippocampal neurons stimulated with EGF. (A) Heatmap of Pearson correlations and correlation plots for the different replicates in the EGF-stimulated and control samples showing high quantititave reproducibility between all measurements. (B) Volcano plot displaying the differential phosphosites observed for control versus EGF-stimulated hippocampal neurons with the significantly regulated phosphosites using a FDR of 5% in dark gray. (C) Observed regulation of the MAPK pathway in EGF-stimulated cells. The sites are colored according to their ratio between the EGF-stimulated and control neurons. Two phosphosites of the mGluR5 receptor are regulated, hinting at communication between EGFR and mGluR5.

dilution series ranging from 1 to 25 μg, prepared from a pooled neuronal protein extract. With only 25 μg of input material, an average of 3615 phosphopeptides could be identified, and by starting with 1 μg of material we could still identify 1963 unique phosphopeptides (Figure 3B). Cumulatively, 2926 class I phosphosites were quantified in at least two replicates for 25 μg starting material and 1098 for 1 μg. Comparable to the HeLa cell digest, we observed a high overlap between the different protein digest amounts, with 98% of the phosphopeptides in the 25 μg sample identified in the samples using lower peptide amounts, as well as high correlations at the label-free quantitative level (Figure S2C). As expected, when comparing equal amounts of protein digest from either HeLa or neuronal cells, we found a lower number of phosphorylated peptides in the neuron samples.

To inspect the dynamic range of the enrichment method in combination with LC-MS/MS analysis, we plotted the normalized MS signal intensities observed for the samples derived from different quantities of protein digest, for both the HeLa and neuron samples, as shown in Figure S4A–D. For both sample types the detectable dynamic range was substantially smaller for the lower sample amounts, suggesting that with less protein digest more high abundant phosphopeptides are being enriched and detected. As shown in Figure S4E,S4F, indeed an overrepresentation of phosphopeptides with high ion intensities is observed. Together, these two data sets demonstrate that even with low quantities of material (down to 1 μg) one can already identify and quantify thousands of phosphorylated peptides in a reliable manner.

To further assess the performance of the automated workflow in quantitative phosphoproteome profiling, we

DOI: 10.1021/acs.jproteome.6b00753
J. Proteome Res. 2017, 16, 728–737

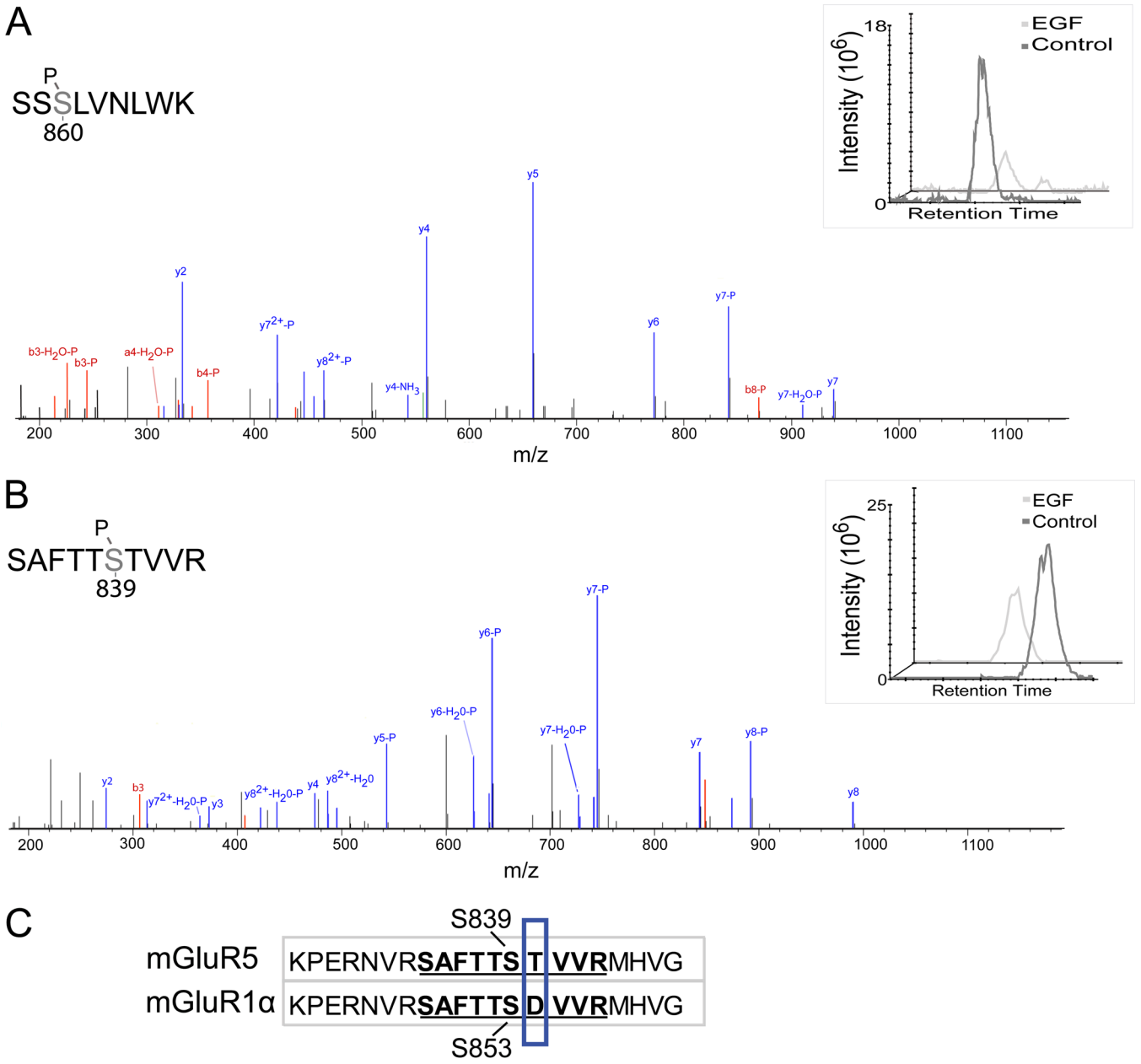

Figure 5. Specific phosphosites of the rat neuron mGluR5 and mGluR1α decreasing phosphorylation upon EGF stimulation. Representative HCD spectra of the mGlur5 peptide phosphorylated at S860 (A) and mGluR5 peptide phosphorylated at S839 (B). The insets show the representative extracted ion chromatogram (XIC) of the phosphorylated peptide in a control and EGF-stimulated sample, displaying the decrease in phosphorylation upon EGF stimulation. (C) Sequence alignment of the mGlur5 and MGlur1α receptor. The sequences of both receptors around S839 and S853 phosphosites are similar (difference is indicated by the blue box around the specific amino acids), and the same trend in phosphorylation was observed upon stimulation with EGF. The phosphopeptides identified in the LC−MS/MS experiment are underlined and highlighted in bold.

mapped the phosphorylation dynamics in primary rat hippocampal neurons upon stimulation with EGF (Figure 1C). The EGF receptor is expressed in hippocampal neurons and found to modulate excitatory synaptic transmission.[33,34] We stimulated hippocampal neurons with 10 ng/mL EGF for 20 min and quantitatively monitored changes in the phosphorylation profiles compared with control, vehicle-treated neurons. A six-well plate format was used where we treated single wells in triplicate, resulting in a maximum of 50 μg of protein input material for the Fe(III)-IMAC phosphopeptide enrichment. From these phosphopeptide enrichments we subjected 40% to single LC−MS/MS gradient of 100 min, resulting in the identification of 6095 unique phosphopeptides from which 4611 class I phosphosites could be quantified in at least two replicates. We assessed the quality of this experiment by plotting Pearson correlations of the EGF and control samples (Figure 4a), showing high quantitative reproducibility, comparable to the first experiment with the nonstimulated neuron samples. Notably, the Pearson correlations of the EGF-treated neurons increased compared with the untreated samples, respectively, >0.98 and >0.83, likely the consequence of synchronization of phosphorylation events in the stimulated neurons in response to EGF. A two-sample t test revealed 603 significantly regulated phosphosites at a FDR of 5% (Figure

DOI: 10.1021/acs.jproteome.6b00753
J. Proteome Res. 2017, 16, 728−737

4B). EGF is known to influence the phosphorylation status of proteins belonging to the MAPK pathway, of which multiple members could be quantified with this method. Indeed, many of these proteins were found to be strongly regulated following EGF stimulation (Figure 4C). Moreover, it has been reported that EGF receptor (EGFR) stimulation in hippocampal neurons enhances NMDA receptor (NMDAR) surface expression and NMDAR-mediated calcium influx, facilitating long-term potentiation (LTP) of synaptic transmission.[33,35] Therefore, we also examined our data for phosphorylation dynamics related to these events. Strikingly, the enrichment method applied here was sensitive enough to detect changes in receptor phosphorylation status, even though the experiment was performed with these low sample amounts. For instance, the known phosphosite S886 in the GluN2B subunit of NMDAR[36,37] was significantly elevated upon EGF treatment. On the contrary, phosphorylation of two sites in the metabotropic glutamate receptor mGluR5, S860 and S839, were significantly down-regulated (Figures 4C and 5A,B). It is known that S839 phosphorylation is required for mGluR5-triggered calcium oscillations,[38] suggesting that EGFR activation can modulate mGluR5-mediated calcium signaling. Furthermore, we observed decreased phosphorylation of S853 on the glutamate receptor mGluR1α. If the sequences of mGluR5 and mGluR1α are aligned, both S839 and S853 show alike motifs;[38] (Figure 5C) therefore, similar behavior of these phosphosites might be expected. It has previously been shown that regulation of mGluR5 by an agonist influences the phosphorylation status of the EGFR in rat cortical astrocytes and striatal neurons, although the link was so far mainly shown via tyrosine kinase signaling.[39,40] Here we observed that EGFR stimulation also influences the phosphorylation status of mGluR5, suggesting that these receptors can influence each other's activity reciprocally (Figure 4C). Of note, besides the hippocampal neurons, our samples also contain a small percentage of supporting glia cells, which are cotransferred during the plating of the neurons. Because EGFR expression in glia cells is considerably more abundant than in neurons, a potential direct or indirect role in the observed EGF response in our neuronal cultures cannot be excluded. Together, these results indicate that a detailed analysis of neuronal protein phosphorylation is feasible, even with limited amounts of input material, and it would be interesting to apply this technique to study the temporal regulation of protein phosphorylation of neuronal proteins involved in synaptic transmission and plasticity.

CONCLUSIONS

So far in MS-based phosphoproteomics, a good coverage of the phosphoproteome relied very much on sample availability. Moreover, current workflows in phosphoproteomics are limited in reproducibility. As the tendency in phosphoproteomics is shifting toward the analysis of more clinically relevant samples, such as (patient-derived) primary cells, organoids, and FACS sorted cells or microdissected from tissue, more sensitive and more robust methods are needed that enable high reproducibility. Here we assessed an automated and miniaturized enrichment protocol using Fe(III)-IMAC cartridges on a AssayMAP Bravo platform and found it to provide an efficient, sensitive, and reproducible approach for phosphoproteomic analysis. We demonstrate reproducible enrichment of thousands of phosphorylated peptides in a qualitative and quantitative manner from a limited amount of digest, even down to the submicrogram level. The potential of this workflow was demonstrated by our quantitative analysis of the phosphorylation dynamics in EGF-stimulated rat hippocampal neurons, using material from single wells containing approximately 200 000 neuron cells. Our highly sensitive and automated phosphoproteomics experiment highlighted, besides proteins in the MAP kinase pathway, EGF-regulated functional phosphosites on several membrane incorporated glutamate receptors.

ASSOCIATED CONTENT

Supporting Information

The Supporting Information is available free of charge on the ACS Publications website at DOI: 10.1021/acs.jproteome.6b00753.

Percentage of S, T, and Y phosphorylation and phosphosite multiplicity of the three different enrichment methods; label-free quantitative phosphoproteome analysis of HeLa/neuron digests using variable amounts of starting material; dynamic range in the phosphoproteome can be extended by using more starting material; and linearity of the quantitative phosphopeptide enrichment by automated Fe(III)-IMAC enrichment. (PDF)

AUTHOR INFORMATION

Corresponding Author

*E-mail: m.altelaar@uu.nl.

ORCID

Albert J. R. Heck: 0000-0002-2405-4404

A. F. Maarten Altelaar: 0000-0001-5093-5945

Author Contributions

‖H.P. and R.P. contributed equally to the work.

Notes

The authors declare no competing financial interest.

Mass spectrometry proteomics data have been deposited to the ProteomeXchange Consortium via the PRIDE partner repository with the data set identifier PXD005366 raw files of all mass spectrometry runs.

ACKNOWLEDGMENTS

A.F.M.A. is supported by The Netherlands Organization for Scientific Research (NWO) through a VIDI grant (723.012.102). This work was partly supported by the *Proteins@Work*, a program of The Netherlands Proteomics Centre financed by The Netherlands Organisation for Scientific Research (NWO) as part of the National Roadmap Large-scale Research Facilities of The Netherlands (project number 184.032.201). This project also received funding from the European Union's Horizon 2020 research and innovation programme (grant agreement MSMed No. 686547) and 7th framework programme (grant agreement Manifold No. 317371).

REFERENCES

(1) Pagel, O.; Loroch, S.; Sickmann, A.; Zahedi, R. P. Current strategies and findings in clinically relevant post-translational modification-specific proteomics. *Expert Rev. Proteomics* **2015**, *12*, 235−253.

(2) Zhou, H.; Di Palma, S.; Preisinger, C.; Peng, M.; Polat, A. N.; Heck, A. J.; Mohammed, S. Toward a comprehensive characterization

of a human cancer cell phosphoproteome. *J. Proteome Res.* **2013**, *12*, 260−271.
(3) Hunter, T. Protein kinases and phosphatases: the yin and yang of protein phosphorylation and signaling. *Cell* **1995**, *80*, 225−236.
(4) Ubersax, J. A.; Ferrell, J. E., Jr. Mechanisms of specificity in protein phosphorylation. *Nat. Rev. Mol. Cell Biol.* **2007**, *8*, 530−541.
(5) Hunter, T. Tyrosine phosphorylation: thirty years and counting. *Curr. Opin. Cell Biol.* **2009**, *21*, 140−146.
(6) Pawson, T.; Scott, J. D. Protein phosphorylation in signaling–50 years and counting. *Trends Biochem. Sci.* **2005**, *30*, 286−290.
(7) Altelaar, A. F.; Munoz, J.; Heck, A. J. Next-generation proteomics: towards an integrative view of proteome dynamics. *Nat. Rev. Genet.* **2012**, *14*, 35−48.
(8) Riley, N. M.; Coon, J. J. Phosphoproteomics in the Age of Rapid and Deep Proteome Profiling. *Anal. Chem.* **2016**, *88*, 74−94.
(9) Matheron, L.; van den Toorn, H.; Heck, A. J.; Mohammed, S. Characterization of biases in phosphopeptide enrichment by Ti(4+)-immobilized metal affinity chromatography and TiO2 using a massive synthetic library and human cell digests. *Anal. Chem.* **2014**, *86*, 8312−8320.
(10) Mann, M.; Ong, S. E.; Gronborg, M.; Steen, H.; Jensen, O. N.; Pandey, A. Analysis of protein phosphorylation using mass spectrometry: deciphering the phosphoproteome. *Trends Biotechnol.* **2002**, *20*, 261−268.
(11) Giansanti, P.; Aye, T. T.; van den Toorn, H.; Peng, M.; van Breukelen, B.; Heck, A. J. An Augmented Multiple-Protease-Based Human Phosphopeptide Atlas. *Cell Rep.* **2015**, *11*, 1834−1843.
(12) Sharma, K.; D'Souza, R. C.; Tyanova, S.; Schaab, C.; Wisniewski, J. R.; Cox, J.; Mann, M. Ultradeep human phosphoproteome reveals a distinct regulatory nature of Tyr and Ser/Thr-based signaling. *Cell Rep.* **2014**, *8*, 1583−1594.
(13) Batth, T. S.; Francavilla, C.; Olsen, J. V. Off-line high-pH reversed-phase fractionation for in-depth phosphoproteomics. *J. Proteome Res.* **2014**, *13*, 6176−6186.
(14) Gauci, S.; Helbig, A. O.; Slijper, M.; Krijgsveld, J.; Heck, A. J.; Mohammed, S. Lys-N and trypsin cover complementary parts of the phosphoproteome in a refined SCX-based approach. *Anal. Chem.* **2009**, *81*, 4493−4501.
(15) Beausoleil, S. A.; Jedrychowski, M.; Schwartz, D.; Elias, J. E.; Villen, J.; Li, J.; Cohn, M. A.; Cantley, L. C.; Gygi, S. P. Large-scale characterization of HeLa cell nuclear phosphoproteins. *Proc. Natl. Acad. Sci. U. S. A.* **2004**, *101*, 12130−12135.
(16) Nuhse, T. S.; Stensballe, A.; Jensen, O. N.; Peck, S. C. Large-scale analysis of in vivo phosphorylated membrane proteins by immobilized metal ion affinity chromatography and mass spectrometry. *Mol. Cell. Proteomics* **2003**, *2*, 1234−1243.
(17) Giansanti, P.; Stokes, M. P.; Silva, J. C.; Scholten, A.; Heck, A. J. Interrogating cAMP-dependent kinase signaling in Jurkat T cells via a protein kinase A targeted immune-precipitation phosphoproteomics approach. *Mol. Cell. Proteomics* **2013**, *12*, 3350−3359.
(18) Pandey, A.; Podtelejnikov, A. V.; Blagoev, B.; Bustelo, X. R.; Mann, M.; Lodish, H. F. Analysis of receptor signaling pathways by mass spectrometry: identification of vav-2 as a substrate of the epidermal and platelet-derived growth factor receptors. *Proc. Natl. Acad. Sci. U. S. A.* **2000**, *97*, 179−184.
(19) Larsen, M. R.; Thingholm, T. E.; Jensen, O. N.; Roepstorff, P.; Jorgensen, T. J. Highly selective enrichment of phosphorylated peptides from peptide mixtures using titanium dioxide microcolumns. *Mol. Cell. Proteomics* **2005**, *4*, 873−886.
(20) Pinkse, M. W.; Uitto, P. M.; Hilhorst, M. J.; Ooms, B.; Heck, A. J. Selective isolation at the femtomole level of phosphopeptides from proteolytic digests using 2D-NanoLC-ESI-MS/MS and titanium oxide precolumns. *Anal. Chem.* **2004**, *76*, 3935−3943.
(21) Andersson, L.; Porath, J. Isolation of phosphoproteins by immobilized metal (Fe3+) affinity chromatography. *Anal. Biochem.* **1986**, *154*, 250−254.
(22) Posewitz, M. C.; Tempst, P. Immobilized gallium(III) affinity chromatography of phosphopeptides. *Anal. Chem.* **1999**, *71*, 2883−2892.
(23) Aryal, U. K.; Olson, D. J.; Ross, A. R. Optimization of immobilized gallium (III) ion affinity chromatography for selective binding and recovery of phosphopeptides from protein digests. *J. Biomol. Technol.* **2008**, *19*, 296−310.
(24) Zhou, H.; Ye, M.; Dong, J.; Han, G.; Jiang, X.; Wu, R.; Zou, H. Specific phosphopeptide enrichment with immobilized titanium ion affinity chromatography adsorbent for phosphoproteome analysis. *J. Proteome Res.* **2008**, *7*, 3957−3967.
(25) Zhou, H.; Ye, M.; Dong, J.; Corradini, E.; Cristobal, A.; Heck, A. J.; Zou, H.; Mohammed, S. Robust phosphoproteome enrichment using monodisperse microsphere-based immobilized titanium (IV) ion affinity chromatography. *Nat. Protoc.* **2013**, *8*, 461−480.
(26) de Graaf, E. L.; Giansanti, P.; Altelaar, A. F.; Heck, A. J. Single-step enrichment by Ti4+-IMAC and label-free quantitation enables in-depth monitoring of phosphorylation dynamics with high reproducibility and temporal resolution. *Mol. Cell. Proteomics* **2014**, *13*, 2426−2434.
(27) Humphrey, S. J.; Azimifar, S. B.; Mann, M. High-throughput phosphoproteomics reveals in vivo insulin signaling dynamics. *Nat. Biotechnol.* **2015**, *33*, 990−995.
(28) Abelin, J. G.; Patel, J.; Lu, X.; Feeney, C. M.; Fagbami, L.; Creech, A. L.; Hu, R.; Lam, D.; Davison, D.; Pino, L.; Qiao, J. W.; Kuhn, E.; Officer, A.; Li, J.; Abbatiello, S.; Subramanian, A.; Sidman, R.; Snyder, E. Y.; Carr, S. A.; Jaffe, J. D. Reduced-representation phosphosignatures measured by quantitative targeted MS capture cellular states and enable large-scale comparison of drug-induced phenotypes. *Mol. Cell. Proteomics* **2016**, *15*, 1622−41.
(29) Frost, N. A.; Shroff, H.; Kong, H.; Betzig, E.; Blanpied, T. A. Single-molecule discrimination of discrete perisynaptic and distributed sites of actin filament assembly within dendritic spines. *Neuron* **2010**, *67*, 86−99.
(30) Kulak, N. A.; Pichler, G.; Paron, I.; Nagaraj, N.; Mann, M. Minimal, encapsulated proteomic-sample processing applied to copy-number estimation in eukaryotic cells. *Nat. Methods* **2014**, *11*, 319−324.
(31) Yu, L. R.; Zhu, Z.; Chan, K. C.; Issaq, H. J.; Dimitrov, D. S.; Veenstra, T. D. Improved titanium dioxide enrichment of phosphopeptides from HeLa cells and high confident phosphopeptide identification by cross-validation of MS/MS and MS/MS/MS spectra. *J. Proteome Res.* **2007**, *6*, 4150−4162.
(32) Montoya, A.; Beltran, L.; Casado, P.; Rodriguez-Prados, J. C.; Cutillas, P. R. Characterization of a TiO(2) enrichment method for label-free quantitative phosphoproteomics. *Methods* **2011**, *54*, 370−378.
(33) Tang, Y.; Ye, M.; Du, Y.; Qiu, X.; Lv, X.; Yang, W.; Luo, J. EGFR signaling upregulates surface expression of the GluN2B-containing NMDA receptor and contributes to long-term potentiation in the hippocampus. *Neuroscience* **2015**, *304*, 109−121.
(34) Tucker, M. S.; Khan, I.; Fuchs-Young, R.; Price, S.; Steininger, T. L.; Greene, G.; Wainer, B. H.; Rosner, M. R. Localization of immunoreactive epidermal growth factor receptor in neonatal and adult rat hippocampus. *Brain Res.* **1993**, *631*, 65−71.
(35) Abe, K.; Saito, H. Epidermal growth factor selectively enhances NMDA receptor-mediated increase of intracellular Ca2+ concentration in rat hippocampal neurons. *Brain Res.* **1992**, *587*, 102−108.
(36) Lundby, A.; Secher, A.; Lage, K.; Nordsborg, N. B.; Dmytriyev, A.; Lundby, C.; Olsen, J. V. Quantitative maps of protein phosphorylation sites across 14 different rat organs and tissues. *Nat. Commun.* **2012**, *3*, 876.
(37) Ghafari, M.; Hoger, H.; Keihan Falsafi, S.; Russo-Schlaff, N.; Pollak, A.; Lubec, G. Mass spectrometrical identification of hippocampal NMDA receptor subunits NR1, NR2A-D and five novel phosphorylation sites on NR2A and NR2B. *J. Proteome Res.* **2012**, *11*, 1891−1896.
(38) Kim, C. H.; Braud, S.; Isaac, J. T.; Roche, K. W. Protein kinase C phosphorylation of the metabotropic glutamate receptor mGluR5 on Serine 839 regulates Ca2+ oscillations. *J. Biol. Chem.* **2005**, *280*, 25409−25415.

DOI: 10.1021/acs.jproteome.6b00753
J. Proteome Res. 2017, 16, 728−737

(39) Peavy, R. D.; Chang, M. S.; Sanders-Bush, E.; Conn, P. J. Metabotropic glutamate receptor 5-induced phosphorylation of extracellular signal-regulated kinase in astrocytes depends on transactivation of the epidermal growth factor receptor. *J. Neurosci.* **2001**, *21*, 9619−9628.
(40) Yang, L.; Mao, L.; Chen, H.; Catavsan, M.; Kozinn, J.; Arora, A.; Liu, X.; Wang, J. Q. A signaling mechanism from G alpha q-protein-coupled metabotropic glutamate receptors to gene expression: role of the c-Jun N-terminal kinase pathway. *J. Neurosci.* **2006**, *26*, 971−980.

DOI: 10.1021/acs.jproteome.6b00753
J. Proteome Res. 2017, 16, 728−737